ARTICLE

Photodissociation Dynamics of Nitromethane and Nitroethane at 266 nm†

Xian-fang Yue, Ju-long Sun, Qiang Wei, Hong-ming Yin, Ke-li Han*

State Key Laboratory of Molecular Reaction Dynamics, Dalian Institute of Chemical Physics, Chinese Academy of Sciences, Dalian 116023, China

(Dated: Received on May 30, 2007; Accepted on July 10, 2007)

Measurements of the nascent OH product from photodissociation of gaseous nitromethane and nitroethane at 266 nm were performed using the single-photon laser induced fluorescence technique. The OH fragment is found to be vibrationally cold for both systems. The rotational state distribution of nitromethane are Boltzmann, with rotational temperature of $T_{\rm rot}$=2045±150 and 1923±150 K for both $^2\Pi_{3/2}$ and $^2\Pi_{1/2}$ states, respectively. For nitroethane, the rotational state distribution shows none Boltzmann and cannot be well characterized by a rotational temperature, which indicates the different mechanisms in producing OH radicals from photodissociation of nitromethane and nitroethane. The rotational energy is calculated as 14.36±0.8 and 4.98±0.8 kJ/mol for nitromethane and nitroethane, respectively. A preferential population of the low spin-orbit component ($^2\Pi_{3/2}$) is observed for both nitromethane and nitroethane. The dominant population of Π^+ state in two Λ-doublet states is also observed for both nitromethane and nitroethane, which indicates that the unpaired π lobe of the OH fragment is parallel to the plane of rotation.

Key words: Photodissociation dynamics, Single-photon laser induced fluorescence, Nitromethane, Nitroethane

I. INTRODUCTION

Nitro-containing compounds play a significant role in propellant ignition, combustion, and atmosphere pollution [1]. Their physical and chemical properties have attracted much interest from scientists due to these important aspects. Experimental and theoretical studies have been extensively performed in the past [2-11].

Nitromethane (CH_3NO_2), the simplest nitroalkane, is one of the most prototypical systems for mechanistic studies because it exhibited complicated multichannel dissociation processes on both the ground and excited electronic states. The ultraviolet absorption spectrum of CH_3NO_2 consists of two bands: a weak band centered at 270 nm and a much stronger band centered at 198 nm. The weak band at 270 nm has long been assigned as a $\pi^*\leftarrow n$ transition, involving promotion of a nonbonding electron of O [12]. The strong band at 198 nm was first observed by Nagakura and assigned as a $\pi^*\leftarrow\pi$ transition localized on the NO_2 moiety [13]. The photodissociation dynamics of CH_3NO_2 have been extensively investigated on both two absorption bands, respectively. The observed photoproducts can be attributed to the following four major channels:

$$CH_3NO_2+h\nu \rightarrow CH_3+NO_2 \quad (1)$$

$$CH_3NO_2+h\nu \rightarrow CH_2O+HNO \quad (2)$$

$$CH_3NO_2+h\nu \rightarrow CH_3O+NO \quad (3)$$

$$CH_3NO_2+h\nu \rightarrow CH_3NO+O \quad (4)$$

Briefly, the results of these studies are presented as follows. On the second absorption band of $\pi^*\leftarrow\pi$ transition, several groups [14-18] have studied the photodissociation of nitromethane at 193, 200, and 218 nm, respectively. One consistent result was formed from these investigations that the primary photodissociation pathway is cleavage of the C−N bond to produce CH_3 and NO_2 with the first electronically excited state $\widetilde{A}^2B_2$, some of which with sufficient internal energy could then dissociate into NO+O. Another minor photolysis channel to produce CH_3 and the ground electronically state NO_2 ($\widetilde{X}^2A_1$) has been proposed by Butler *et al.* with fluorescence emission spectroscopy and photofragment translational spectroscopy technique [15], and NO_2 ($\widetilde{X}^2A_1$) could absorb another 193 nm photon to dissociate into NO+O. Further studies by Lao *et al.* [16] and Moss *et al.* [17] have reached the consistent results with Butler *et al.* and then confirmed the proposed photodissociation mechanism for the minor channel [15]. Unfortunately, studies of the photodissociation of CH_3NO_2 following excitation of the weak $\pi^*\leftarrow n$ transition have produced less consistent results. The ground and vibrationally excited state of NO_2 product were observed in the photodissociation of CH_3NO_2 at 252.6 nm by Spears *et al.* [19] and 264 nm by Schoen *et al.* [20]. However, no photodissociation was observed by Kwok *et al.* in the photodissociation of CH_3NO_2 at 266 nm under collision-free conditions [21]. A small yield of OH radicals was observed by Zabarnick *et al.* in the 266 nm photodissociation of CH_3NO_2 under collision-free conditions [22], but no OH product was observed by Greenblatt *et al.* at 282 nm photolysis of CH_3NO_2 [23].

In contrast to the number of experimental studies of CH_3NO_2, theoretical work on this system was rather

†Part of the special issue "Cun-hao Zhang Festschrift".

*Author to whom correspondence should be addressed. E-mail: klhan@dicp.ac.cn

little. Several groups have calculated the ground state potential energy surface (PES) and the thermal decomposition of nitromethane [25-28]. Corresponding calculations on the excited state PESs photodissociation have also been carried out [29-32]. Arenas *et al.* calculated the excited state PESs and 193 nm photodissociation of CH_3NO_2 [31-32], two dissociation channels were proposed: a major channel consisting of excitation to the $2A''$ state, internal conversion to the $2A'$ state, and dissociation to produce CH_3+NO_2 ($\widetilde{B}^2B_1$), and a minor channel where the initially excited $2A''$ state directly dissociates to produce CH_3+NO_2 ($\widetilde{C}^2A_2$). Their more recent work [32] proposes a radiationless decay through a conical intersection, which deactivates the electronically excited nitromethane and causes it to dissociate and form CH_3+NO_2 ($\widetilde{A}^2B_2$), which is consistent with the assignments of Butler *et al.* [15].

Analogous dissociation channels are possible for the higher alkanes. Howerver, very limited information is available in literature regarding the photodissociation of nitroalkanes with two or more carbon atoms. For nitroethane, $CH_3CH_2NO_2$, its UV absorption spectrum consists of two smooth, broad bands centered roughly at 280 and 200 nm [33]. The band at longer wavelength has been assigned to a $\pi^*\leftarrow n$ transition that is located on the NO_2 functional group, while the feature at 200 nm is assigned to a $\pi^*\leftarrow\pi$ transition also located on the NO_2 chromophore [13]. In the first absorption band, our group studied the photodissociation dynamics of gaseous $CH_3CH_2NO_2$ at 266 nm by monitoring the NO product using single-photon LIF technique [34]. Greenblatt *et al.* observed the OH product from the 282 nm photodissociation of $CH_3CH_2NO_2$ under collision-free conditions. Other UV photodecomposition is less studied.

For nitroalkanes, the dissociation mechanisms are quite complicated due to the large number of energetically allowed product decay channels. There is still no clear picture of the dissociation emerged until now. Further studies on these systems are needed. In this work, the photodissociation of nitromethane and nitroethane at 266 nm was investigated with focus on the detection of nascent OH product from the photolysis. A detailed analysis of the quantum state distributions of the nascent OH fragments were presented.

II. EXPERIMENTS

The experimental apparatus used in the present study has been described in detail elsewhere [35,36]. Briefly, the second-harmonic output of a Nd:YAG laser (Spectra-Physics, GCR-170, 10 Hz) was used to pump a dye laser (Lumonics, HD-500), which generate the tunable laser pulses. The output of the dye laser was then introduced into a Harmonic Generator (Lumonics, HT-1000) to produce the frequency-doubled laser pulses, and which was used for the probe laser pulses. The residual part of the 1064 nm output of the Nd:YAG laser was converted into 266 nm (3-4 ns duration) by a KD*P crystal and provided the photolysis pulses. Both the photolysis and probe beams were counterpropagated and softly focused on the center of the photolysis cell. The probe pulse was optically delayed with respect to the photolysis pulse by ∼15 ns. This delay period was sufficient to separate the two laser pulses, and was short enough to make collision effects negligible under the pressure (typically 26 Pa) used in the experiments.

The fluorescence was collected by a photomultiplier tube (PMT) (Hamamatsu, CR161). A suitable band pass filter was placed in front of the PMT to cut off scattering from the photolysis-laser and probe-laser. The signal was gate-integrated by a Boxcar (SRS, SR250), A/D converted by a homemade interface, and stored in a personal computer using a data-taking program. The linearity of the LIF signal with the pressure of the sample, the probe laser intensity, and the photolysis laser intensity were carefully checked. The LIF spectra were recorded at least three times to ensure a proper signal was obtained.

Nitromethane (Aldrich, ≥99%) and Nitroethane (Aldrich, ≥99%) were purchased in commerce and used without further purification. Helium carrier gas was bubbled through the sample and the gas mixture was expanded into the photolysis cell.

III. RESULTS AND DISCUSSION

The photodissociation of gaseous nitromethane and nitroethane has been carried out using the single-photon laser induced fluorescence technique under bulk conditions at room temperature at 266 nm. The OH photoproducts were unambiguously identified by their characteristic LIF spectrum in the 306-316 nm region due to the $X^2\Pi$ (v''=0)→$A^2\Sigma^+$ (v'=0) transition. Figure 1 (a) and (c) display a typical experimental spectrum of this band for CH_3NO_2 and $CH_3CH_2NO_2$, respectively. The internal state distributions are not accurately deducible directly from the raw experimental line intensities due to the problem of overlapping fine-structure doublets. The effective method to solve this problem is to compare the experimental spectra with the simulated ones calculated from the known spectroscopic constants [37]. The intensities of the fluorescence signal (I_F) are related to the populations of a ground rovibrational state $N(J'',v'')$ by the expression:

$$I_F \propto \frac{N(J'', v'')q_{v'v''}S_{J'J''}f(\nu, \nu_0)}{(2J''+1)} \tag{5}$$

where $q_{v'v''}$ are the known Franck-Condon factors for the OH A-X transition [37], $S_{J'J''}$ are the line strengths for the OH A-X one-photon rotational transitions [38], and $f(\nu,\nu_0)$=$\rho(\nu_0)$exp$[-a(\nu-\nu_0)^2]$ is the laser intensity function. For comparison, Figure 1 (b) and (d) display the simulated spectrum of OH(0,0) band.

DOI:10.1088/1674-0068/20/04/401-406

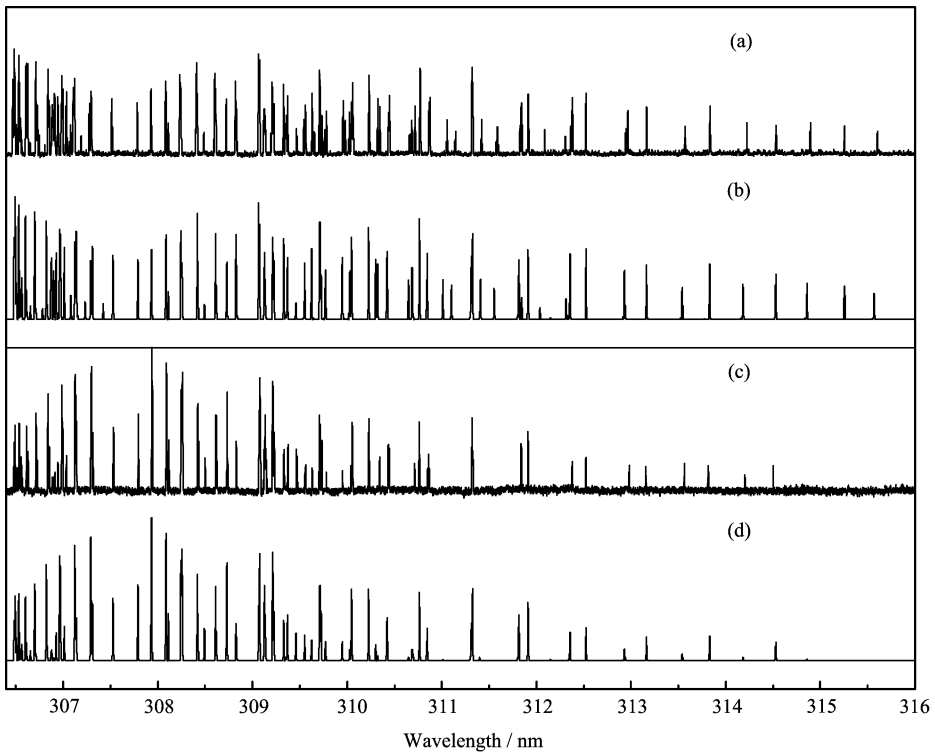

FIG. 1 A portion of the $A^2\Sigma^+$ (v'=0)←$X^2\Pi$ (v''=0) band of the single-photon LIF spectrum of the nascent OH fragment from the photodissociation of nitromethane and nitroethane at 266 nm. (a) experimental spectrum for CH_3NO_2, (b) simulation spectrum for CH_3NO_2, (c) experimental spectra for $CH_3CH_2NO_2$, (d) simulation spectrum for $CH_3CH_2NO_2$.

The OH transitions are labeled following Hund's case (a). The P, Q, or R branches are for the cases of ΔJ or ΔN=−1, 0, or 1, respectively. The subscript 1 or 2 represent $^2\Pi_{3/2}$ or $^2\Pi_{1/2}$ states, respectively. According to the parity selection rule (+↔−), the Q branches only correspond to the Π^- state, while the P and R branches are attributed to the Π^+ state.

In order to measure the various distributions (rotational, fine structure, and Λ-doublets), the data collection and its subsequent normalization have to be carefully performed. Here, we normalize intensities of the observed LIF rotational lines with respect to the pressure of the sample in the photolysis cell, both the probe and photolysis laser intensities, respectively. The rotational state populations of nascent OH radicals are determined by analyzing the P, Q, and R branches from the $^2\Pi_{3/2}$ and $^2\Pi_{1/2}$ states. The P and R branches probe the same Λ-doublet level (Π^+, A′), and the population obtained from P and R are given for the OH fragment in the Π^+ state. Meanwhile, the Q branch probes the other Λ-doublet level (Π^-, A″), and is used to give the OH population in the Π^- state. From the normalized signals, it is found that the rotational state distributions of the OH fragments (v''=0) are peaked at N=4 and has a long tail up to the highest N=15 for CH_3NO_2, and that the populations can be approximately characterized by "rotational temperature". The equation of the Boltzmann population distribution is expressed as follows:

$$\ln \frac{N(J'')}{(2J''+1)} = \frac{-\varepsilon(J'')hc}{kT_R} + \text{contant} \qquad (6)$$

Figure 2 (a) and (b) show "Boltzmann" plot for the $X^2\Pi_{3/2}$ and $X^2\Pi_{1/2}$ sets of levels from the best linear fit to the experimental data, respectively. The data of the $X^2\Pi_{3/2}$ state was obtained from the sum of distributions from Q_1, P_1, and R_1 branches. Correspondingly, the data of the $X^2\Pi_{1/2}$ state was obtained from the sum of distributions from Q_2, P_2, and R_2 branches. The rotational temperatures calculated from the line slope are 2045±150 and 1923±150 K for the $X^2\Pi_{3/2}$ and $X^2\Pi_{1/2}$ states, respectively. The rotational energy of the ground state $X^2\Pi$ (v''=0) was calculated by $E_{v''}^{\text{rot}}=\sum_{J''} N(J'')\varepsilon(J'')$, where $N(J'')$ is the state distribution and $\varepsilon(J'')$ the energy of a given rotational state, and is found to be 14.36±0.8 kJ/mol.

Correspondingly, the rotational distribution of $X^2\Pi_{3/2}$ and $X^2\Pi_{1/2}$ states of the nascent OH products from photolysis of $CH_3CH_2NO_2$ at 266 nm is also depicted in Fig.3 (a) and (b). It can be seen obviously from Fig.3 that the OH produced from $CH_3CH_2NO_2$ is rotationally much "colder" than that produced from CH_3NO_2. Its highest distribution only attains to N=9. Complicatedly relative to nitromethane, the rotational state distributions can not be characterized by a sim-

DOI:10.1088/1674-0068/20/04/401-406

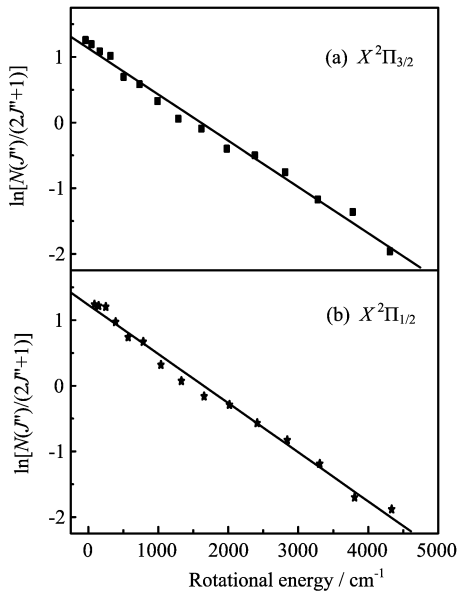

FIG. 2 Boltzmann plots for populations in OH produced from nitromethane photolysis at 266 nm. The solid lines were the best linear fit for the above distributions at rotational temperatures 2045 and 1923 K for (a) and (b), respectively.

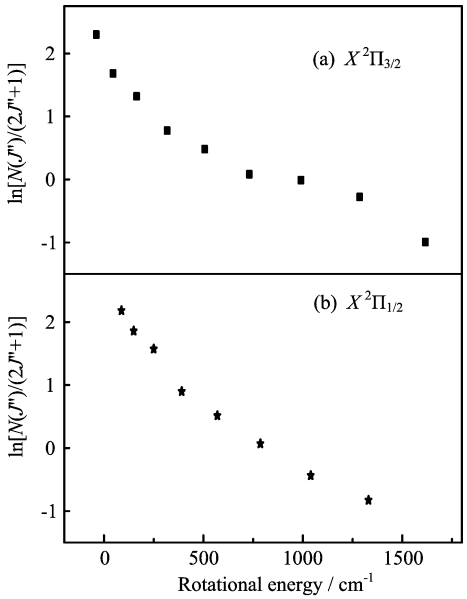

FIG. 3 Plots for populations in OH produced from $CH_3CH_2NO_2$ photolysis at 266 nm.

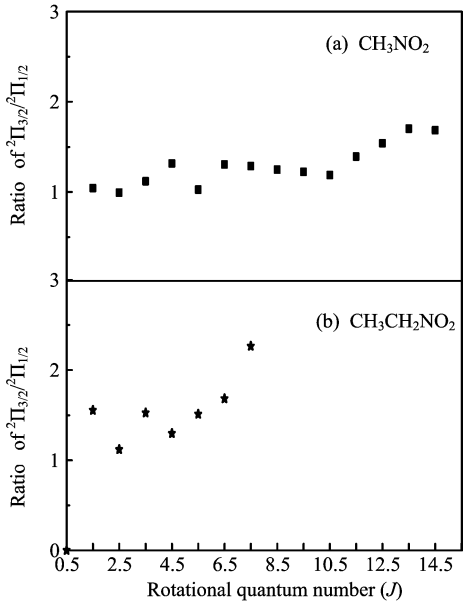

FIG. 4 The ratios of rotational state distributions in the $^2\Pi_{3/2}$ state and $^2\Pi_{1/2}$ state of OH ($X^2\Pi$, v''=0) fragments from the photodissociation at 266 nm.

ple Boltzmann temperature. This result is in consistent with Radhakrishnan's conclusion [39], who studied the photodissociation of 2-nitropropane using one-photon LIF technique at 222, 249, and 355 nm, respectively. The OH and HONO were detected at the same time, and the production of HONO increased with the longer wavelength of the photolysis laser. A number of the nascent HONO will dissociate to NO+OH when their internal energy exceeds 201 kJ/mol [39]. The relative complicated rotational state distribution gives an evidence that the origin of the nascent OH production should come from both the direct and indirect pathway from the photolysis of nitroethane at 266 nm. The rotational energy of ground vibrationally OH product is 4.98±0.8 kJ/mol. On both photodissociation processes of CH_3NO_2 and $CH_3CH_2NO_2$, no OH (v''=1) could be observed, even when using higher photolysis laser power and increasing the probe laser intensity.

The $^2\Pi_{3/2}/^2\Pi_{1/2}$ ratios are plotted against the rotational quantum number J in Fig.4 (a) and (b) for both CH_3NO_2 and $CH_3CH_2NO_2$, respectively. As can be seen from the plot, $^2\Pi_{3/2}$ level seems to be slightly preferential populated. It is interesting to note that the $^2\Pi_{3/2}$ state lies at lower energies due to the inverted spin-orbit coupling of OH radical, the available energy for the OH fragment in the $^2\Pi_{3/2}$ state is lower. Therefore, the rotational state distribution are expected to be slightly shifted to the low J's for the OH fragment in the $^2\Pi_{3/2}$ state compared to that the higher energy spin-orbit state of $^2\Pi_{1/2}$ state. This energetic difference of two spin states could be partly responsible for the ratios of $^2\Pi_{3/2}/^2\Pi_{1/2}$ in Fig.4 (a) and (b).

The Λ-doublet arises from the orientation of pπ lobes of OH with respect to the plane of rotation. In the Π^+ (A′) state, the pπ lobe lies in the plane of rotation, while in the Π^- (A″) state the pπ lobe is perpendicular to the plane of rotation. As mentioned earlier, the Q branches are for the detecting of the OH fragment in the Π^- state, while the R (and P) branches are due to the Π^+ state [40]. The R/Q (or P/Q) intensity ratios represent the ratios of the Λ-doublet, which can

DOI:10.1088/1674-0068/20/04/401-406

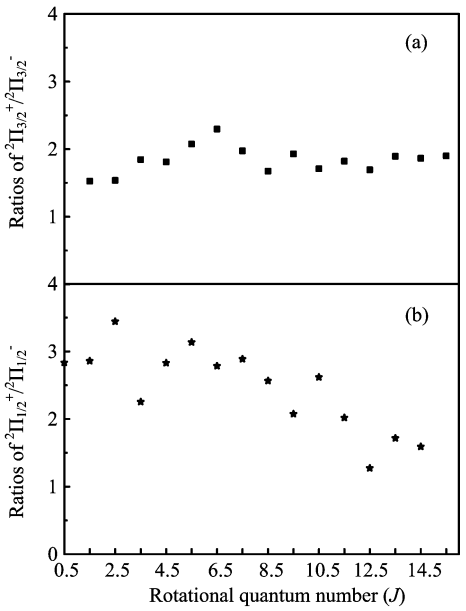

FIG. 5 Ratios of the $^2\Pi_{3/2}$ and $^2\Pi_{1/2}$ states of Λ-doublet populations versus rotational quantum number J for nascent OH ($X^2\Pi$, v''=0) from the photodissociation of CH_3NO_2 at 266 nm.

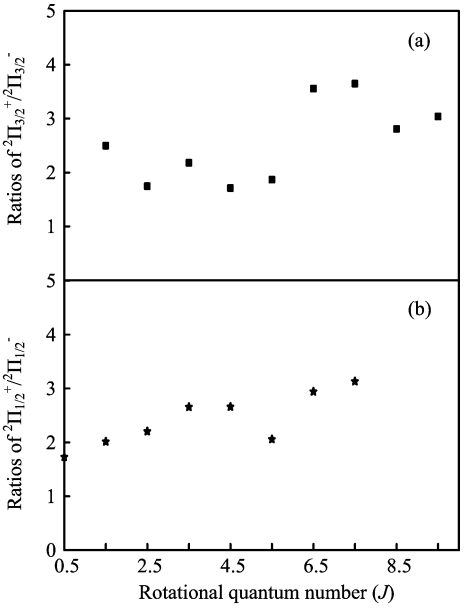

FIG. 6 Ratios of the $^2\Pi_{3/2}$ and $^2\Pi_{1/2}$ states of Λ-doublet populations versus rotational quantum number J for nascent OH ($X^2\Pi$, v''=0) from the photodissociation of $CH_3CH_2NO_2$ at 266 nm.

give information about the relative population of the OH fragment in the Π^+ and Π^- states [36,40]. The ratios of P_1/Q_1 and R_2/Q_2 versus the rotational quantum number J for the $\Pi_{3/2}{}^+/\Pi_{3/2}{}^-$ and $\Pi_{1/2}{}^+/\Pi_{1/2}{}^-$ state are depicted in Fig.5 and Fig.6 for CH_3NO_2 and $CH_3CH_2NO_2$, respectively. The distribution of the Π^+ state is slightly preferential than that of the Π^- state in both of the $\Pi_{3/2}$ and $\Pi_{1/2}$ states, which suggests that the pπ electronic orbital of the OH radical is predominantly parallel to its plane of rotation.

Different rotational state distributions of the nascent OH product from photodissociation of nitromethane and nitroethane imply that different dissociation mechanisms are existed in the two photolysis processes. For $CH_3CH_2NO_2$, a five-membered ring transition sate existed in producing OH product has been proposed by Greenblatt *et al.* [23] with their isotopic substitution photolysis studies. For CH_3NO_2, a four-membered ring transition state is inevitably proposed to produce OH fragments in photodissociation process, just like the calculated transition state by He's group in the ground electronically state [28]. It is obviously that OH products from photodissociation of CH_3NO_2 possess more internal energy and higher rotational state distributions than that from photolysis of $CH_3CH_2NO_2$. The results is in good agreement with the experiments of Zabarnick *et al.*, in which a small yield of OH radicals was observed with 266 nm photolysis of nitromethane [22]. But it is contradictory with the results of Greenblatt *et al.*, that no OH products was observed from nitromethane photolysis at 282 nm [23]. Combining previous studies and our observations, we proposed that there possibly existed a threshold to produce the OH radical from the photolysis of CH_3NO_2 between 266 and 282 nm, and such detailed postulation will be dealt with in future experiments.

IV. CONCLUSION

The photodissociation dynamics of gaseous nitromethane and nitroethane was investigated at 266 nm under bulk conditions at room temperature. The OH production from photolysis of nitromethane and nitroethane was confirmed. The quantum state distributions of the nascent OH fragment was measured using the single-photon LIF technique. Different photodissociation mechanisms of nitromethane and nitroethane was observed indirectly. The OH fragment is found to be vibrationally cold for both systems. The rotational state distribution of OH fragment of nitromethane shows a Boltzmann behavior with $T_{\rm rot}$=2045 ±150 and 1923±150 K for $^2\Pi_{3/2}$ and $^2\Pi_{1/2}$ states, respectively. The relative complicated rotational state distribution of the OH production of nitroethane suggests different dissociation mechanism in contrast to CH_3NO_2. The $^2\Pi_{3/2}$ state is slightly preferential populated than the $^2\Pi_{1/2}$ state of the OH fragment for both nitromethane and nitroethane. The population in the Π^+ state was predominant for two Λ-doublet states for both nitromethane and nitroethane systems.

DOI:10.1088/1674-0068/20/04/401-406

V. ACKNOWLEDGMENTS

This work was supported by the National Natural Science Foundation of China (No.20333050, No.20573110) and the Knowledge Innovation Program of the Chinese Academy of Sciences, Dalian Institute of Chemical Physics (No.K603211A01).

[1] L. Batt and G. N. Robinson, *The Chemistry of Amino, Nitroso and Nitro Compounds and Their Derivatives*, New York: Wiley, Parts 1 and 2, (1982).
[2] A. C. Gonzalez, C. W. Larson, D. F. McMillen, and D. M. Golden, J. Phys. Chem. **89**, 4809 (1985).
[3] M. J. S. Dewar and J. P. J. Ritchie, J. Org. Chem. **50**, 1031 (1985).
[4] W. Tsang, D. Robaugh, and W. G. Mallard, J. Phys. Chem. **90**, 5968 (1986).
[5] R. P. Saxon, J. Phys. Chem. **93**, 3130 (1989).
[6] M. L. Mckee, Chem. Phys. Lett. **164**, 520 (1989).
[7] R. C. Mowrey, M. Page, G. G. Adames, and B. H. Lengsfield, J. Chem. Phys. **93**, 1857 (1990).
[8] T. S. Dibble and J. S. Francisco. J. Phys. Chem. **98**, 5010 (1994).
[9] A. Gindulyte, L. Massa, L. Huang, and J. Karle, J. Phys. Chem. A **103**, 11040 (1999).
[10] R. Bianco and J. T. Hynes, J. Phys. Chem. A **103**, 3797 (1999).
[11] Y. M. Li, J. L. Sun, H. M. Yin, K. L. Han, and G. Z. He, J. Chem. Phys. **118**, 6244 (2003).
[12] N. S. Bayliss and E. G. McRae, J. Phys. Chem. **58**, 1006 (1954).
[13] S. Nagakura, Mol. Phys. **3**, 152 (1960).
[14] N. C. Blais, J. Chem. Phys. **79**, 1723 (1983).
[15] L. J. Butle, D. Krajnovich, Y. T. Lee, G. Ondrey, and R. Bersohn, J. Chem. Phys. **79**, 1708 (1983).
[16] K. Q. Lao, E. Jensen, P. W. Kash, and L. J. Butler, J. Chem. Phys. **93**, 3958 (1990).
[17] D. B. Moss, K. A. Trentelman, and P. L. Houston, J. Chem. Phys. **96**, 237 (1992).
[18] E. A. Wade, K. E. Reak, S. L. Li, S. M. Clegg, P. Zou, and D. L. Osborn, J. Phys. Chem. A **110**, 4405 (2006).
[19] K. J. Spears and S. P. Brugge, Chem. Phys. Lett. **54**, 373 (1978).
[20] P. E. Schoen, M. J. Marrone, J. M. Schnur, and L. S. Goldberg, Chem. Phys. Lett. **90**, 272 (1982).
[21] H. S. Kwok, G. Z. He, R. K. Sparks, and Y. T. Lee, Int. J. Chem. Kinet. **13**, 1125 (1981).
[22] S. Zabarnick, J. W. Fleming, and A. P. Baronavski, J. Chem. Phys. **85**, 3395 (1986).
[23] G. D. Greenblatt, H. Zuckerman, and Y. Haas, Chem. Phys. Lett. **134**, 593 (1987).
[24] M. S. Park, K. H. Jung, H. P. Upadhyaya, and H. R. Volpp, Chem. Phys. Lett. **270**, 133 (2001).
[25] M. J. S. Dewar, J. P. Ritchie, and J. Alster, J. Org. Chem. **50**, 1031 (1985).
[26] M. L. McKee, J. Phys. Chem. **93**, 7365 (1989).
[27] M. T. Nguyen, H. T. Le, B. Hajgato, T. Veszpremi, and M. C. Lin, J. Phys. Chem. A **107**, 4286 (2003).
[28] W. F. He, T. J. He, D. M. Chen, and F. C. Liu, J. Phys. Chem. A **106**, 7294 (2002).
[29] C. Mijoule, S. Odiot, S. Fliszar, and J. M. Schnur, J. Mol. Struct.: Theochem. **149**, 311 (1987).
[30] S. Roszak and J. J. Kaufman, J. Chem. Phys. **94**, 6030 (1991).
[31] J. F. Arenas, J. C. Otero, D. Peláez, and J. Soto, J. Chem. Phys. **119**, 7814 (2003).
[32] J. F. Arenas, J. C. Otero, D. Peláez, and J. Soto, J. Chem. Phys. **122**, 084324 (2005).
[33] H. L. Gregory, Ph.D. Dissertation, University of Wisconsion-Madison, (1992).
[34] Y. M. Li, J. L. Sun, K. L. Han, G. Z. He, and Z. J. Li, Chem. Phys. Lett. **421**, 232 (2006).
[35] H. M.Yin, J. L. Sun, Y. M. Li, K. L. Han, and G. Z. He, J. Chem. Phys. **118**, 8248 (2003).
[36] X. F. Yue, J. L. Sun, Z. F. Liu, Q. Wei, and K. L. Han, Chem. Phys. Lett. **426**, 57 (2006).
[37] J. Luque and D. R. Crosley, J. Chem. Phys. **109**, 439 (1998).
[38] I. Kovacs, *Rotational Structure in the Spectra of Diatomic Molecule*, London: Adam Hilger Ltd., 130 (1969).
[39] G. Radhakrishnan, T. Parr, and C. Wittig, Chem. Phys. Lett. **111**, 25 (1984).
[40] P. Andresen, G. S. Ondrey, B. Titze, and E. W. Rothe, J. Chem. Phys. **80**, 2584 (1984).

DOI:10.1088/1674-0068/20/04/401-406